Modelling of Implantable Photovoltaic Cells Based on Human Skin Types

Jinwei Zhao, Kaung Oo Htet, Rami Ghannam, Muhammad Imran and Hadi Heidari
School of Engineering,
University of Glasgow,
Glasgow, UK
j.zhao.3@research.gla.ac.uk, {Rami.Ghannam, Muhammad.Imran, Hadi.Heidari}@glasgow.ac.uk

***Abstract*—Implantable electronic devices are emerging as important healthcare technologies due to their sustainable operation and low risk of infection. To overcome the drawbacks of the built-in battery in implantable devices, energy harvesting from the human body or another external source is required.. Energy harvesting using appropriately sized and properly designed photovoltaic cells enable implantable medical devices to be autonomous and self-powered. Among the challenges in using PV cells is the small fraction of incident light that penetrates the skin. Thus, it is necessary to involve such physical properties in the energy harvesting system design. Consequently, we propose a novel photodiode model that considers skin loss in different ethnic groups. Our physical simulations have been implemented using COMSOL and MATLAB. Circuit and system modelling has been performed using Cadence 180nm technology. Our results show that the transmittance of near infrared light is almost the same in three skin types: Caucasian, Asian and African. Maximum power delivery of 12 μW (African skin) and 14 μW (Caucasian and Asian skin) were achieved at 0.45 V. With the help of a power management unit, an output voltage of 1.8-2 V was achieved using the PV cells.**

Keywords—Solar power harvesting system, optic analysis, tissue loss and power management.

I. Introduction

As an emerging technology, biomedical implantable devices play a more and more crucial role in the pharmaceutical discovery and life science [1]. The modern therapy and diagnose are sufficiently improved according to the real-time health monitoring and implantable drug pump. The advancement in implantable technology is exploited to avoid the transcutaneous connection and infective risks. However, the powering issue of the implantable device is still a significant challenge because of the limited lifespan of built-in batteries. For instance, the average lifetime of a cardiac pacemaker is 7-10 years, while the lifespan of neurostimulator is 3-5 years [2]. In this case, a surgical battery replacement is required to prolong the usage of implantable device. To overcome this problem, there are lots of powering technologies such as the piezoelectric generator, wireless power transfer coils, thermal-electric generator, biofuel generator and implantable solar power harvester [3-5]. Compared with the other powering topologies, the implantable photovoltaic cell (PV) takes advantages of no external powering unit, sustainable and reliable power output and high output voltage. However, the power generation of implantable PV cell highly dependents on the light irradiance from ambient and tissue loss. When the ambient light penetrates the human tissue, most of the light energy will be absorbed by the skin and only a few effective light energies can be applied by the device. The different skin types corresponding to ethnic, age, gender and different locations of the body should be investigated because they affect the device performance in implantable solar power harvesting. Firstly, we will analyse the physical performance in FEM simulator (COMSOL Multiphysics) and the optic performance in MATLAB. Then the electric profile will be inherited into an model by using Verilog A in Cadence. The advantages of this operation are involving influences of macroscopic device modelling, such as tissue loss, into system level to optimize the device performance in power harvesting system. Power management circuit is presented and consist of start-up circuit and main charge pump to provide a range of operational voltages to multiple implantable applications from the solar harvested low output voltage [6]. The motivation of this paper is to present a self-powered implant system powered by solar harvester which is modelled to closely match the skin of the living organism.

II. Optic and Device Modelling

Fig. 1 shows the design procedure of power harvesting system. Initially, the optic performance is analysed by Jones' matrix in MATLAB. The skin properties are evaluated from skin absorption coefficients in previous studies and the tissue transmittance with vary wavelength spectrum is achieved [7]. In this case, three skin properties in volar forearm according to three ethnic groups (Caucasian, African and Asian) are selected based on the research of Tseng, S.-H., et al. (2008) [7]. The refractive index (N) of human skin is from the research of Bashkatov, A. N., et al. (2011) [8]. We apply the crystalline silicon as the device material because of high power conversion efficiency. The properties of silicon is achieved from Vuye, G., et al. (1993) [9]. The macroscopic device modelling is developed by COMSOL Multiphysics with the setup of doping profile, generation and recombination, geometry, AM1.5G (Air mass 1.5 global) and skin transmittance from MATLAB. The equivalent circuit of implantable PV cells is designed by Cadence with current vs voltage (IV) curve imported from COMSOL simulation. The performance of the power management unit is tested by using the power and voltage output from PV cells.

A. Optic analysis in MATLAB

The 1D structure model is shown in Fig. 1. To simulate the property (reflectance, absorptance and transmittance) of light through tissue, we are using Snell's law. A simplified method invoked representing them is the Jones' Matrix method (M), which is shown in [10, 11]:

$$M = \sum_{i=1}^{q} \begin{bmatrix} \cos\varphi_i & (j/\eta_i)\sin\varphi_i \\ j\eta_i \sin\varphi_i & \cos\varphi_i \end{bmatrix} \quad (1)$$

Where q means the number of layers, and i th layer is indicated by a 2 by 2 matrix. The product of matrices represents the combined optical property of all layers. η is the phase shift of each material ($\eta=N\cos\theta$). In the best condition, we choose the incident angle (θ) as 0, and η will be equal to N. φ is the pseudo index of layers, which is related to layer depth d and wavelength λ ($\varphi_i=2\pi N_i d_i \cos\theta_i/\lambda$). The

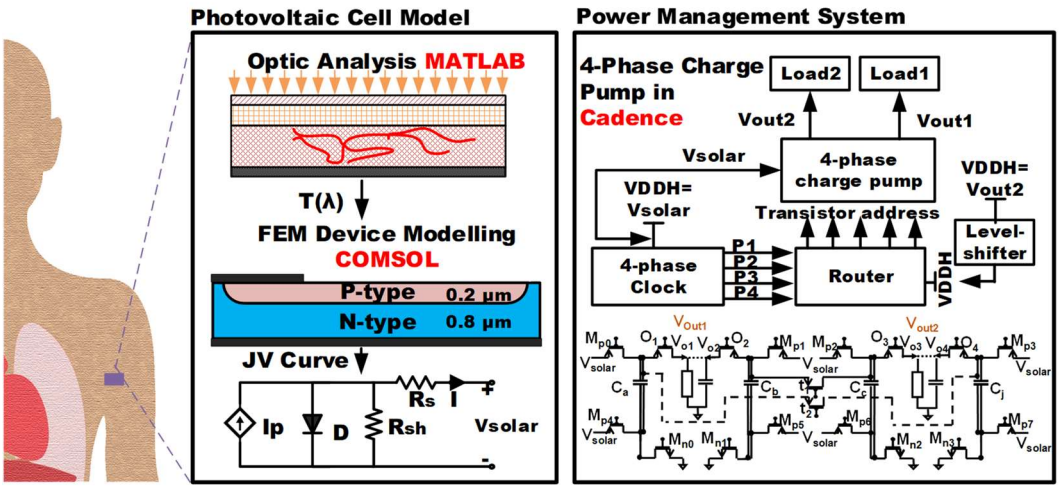

Fig. 1. Design procedure of implantable power harvesting system. Photovoltaic cell model consists of optical analysis, FEM modelling and Cadence modelling. The structure used in optical analysis are composed of: Stratum Corneum, Epidermis and Dermis as well as silicon photodiode. The imported variables T(λ) is transmittance of skin, JV curve is current density to voltage curve. P and V are power and voltage from photodiode respectively. And Power Management in Cadence.

transmittance of multilayer consisting of tissue and silicon PV cell is presented [11]:

$$T = [\frac{2\sqrt{N_{ex}}\eta_{in}}{\sqrt{N_{in}}(\eta_{in}m_{11} + \eta_{ex}m_{22} + \eta_{in}\eta_{ex}m_{12} + m_{21})}]^2 \quad (2)$$

where N is the refractive index of the material, 'ex' represents the exit material and 'in' represents the incidence material.

B. Device Modelling in COMSOL and Cadence

Now turning point to the device simulation in COMSOL, the semiconductor device simulation is based on the Continuity Equation, which is shown in [12]:

$$\frac{\partial n}{\partial t} = \frac{1}{q}\nabla \bullet J_n + G - R$$
$$\frac{\partial p}{\partial t} = -\frac{1}{q}\nabla \bullet J_p + G - R \quad (3)$$

Where n and p are electron and hole concentrations, G and R are the generation and recombination of electron-hole pairs, J_p and J_n are the current density related to holes and electrons respectively, and q is charge density. Periodic boundary conditions were chosen. Carrier transport was modelled by solving the Semiconductor Continuity Equations using FDTD (Finite-Difference Time Domin). The doping profile follows the device in [3]. The short-circuit current density I_{sc} can be achieved by [12]:

$$I_{sc} = A \times \int_{\lambda}\int_{t} J_n(t,\lambda) + J_p(t,\lambda)\, dt d\lambda \quad (4)$$

Where 'A' is the active area of the device, and 't' is the depth of device. To activate this equation in COMSOL. The area is *1 mm*^{2}, which follows the agreement from [13, 14]. When the light penetrates the tissue, the photo-generated current will diminish because most of the energy will be absorbed by human skin. The skin transmittance from the optic analysis is applied to calculate the short-circuit current after tissue loss, which is shown in [3, 12]:

$$I_{sc\,(skin)} = \int_{\lambda=0}^{\infty} T(\lambda) I_{sc}(\lambda)\, d\lambda \quad (5)$$

The IV curve can be expressed as Eq. 6 considering the parasitic resistance [12]:

$$I(V) = I_{sc\,(skin)} - I_d(V) - \frac{V + I(V)R_s}{R_{sh}} \quad (6)$$

From the IV curve, we can deduce important PV cell parameters, such as series resistance (R_s), shunt resistance (R_{sh}), open-circuit voltage (V_{oc}), dark current (I_d) and short-circuit current (I_{sc}). R_s is *0* because the model is 2D, and R_{sh} is obtained using the IV curve to deduce the slope at *0 V*. With these parameters from COMSOL simulation, the equivalent circuit in Cadence can be built up. The parameters in the model are shown in Table 1.

C. Power management in subcutaneous applications

The start-up charge pump [15] or use 2-PV cells in series to boost the low voltage from the solar output 0.9 V input of the main charge pump. The 4-phases rotations series-parallel charge pump has implemented as the main circuit and presented in [16, 17]. This is because this converter can supply the various voltage range of implantable applications at the load ends by only using four integrated capacitors and switches. Moreover, thanks to reconfigurable two different simultaneous voltage outputs, by taking advantage of second output, the peripheral digital circuitry can be potentially self-powered or use it to supply two different loads with different stages without needing to drop down from optimum voltage through low dropped out the circuit and can minimise the power loss across it. Two modes are provided by the 4-phase charge pump, which is double boost mode and supper boost mode. In the double boost mode, the input voltage is doubled in all output ports. In super boost, two of output voltages is tripled from the input and the other two remains doubled.

TABLE I PARAMETERS OF OUR MODEL

Parameter	Value
t_n	0.8 μm
t_p	0.2 μm
N^+	10^{18} cm^{-3}
P^+	10^{20} cm^{-3}
n_i	1.5×10^{10} cm^{-3}
Area	1 mm^2
Cross-section	100 μm^2
R_{sh}	1.5 MΩ

Then interleaved each other since identical amplitude with different phase and get Vout1 and Vout2.

III. Results and Discussion

Initially, the transmittance spectrum of human skin evaluated from MATLAB simulation is shown in Fig. 2 (a). The spectrum range is chosen from *450 nm* to *1000 nm* to check the transmittance in the visible range (*390 nm – 700 nm*) and Near-infrared range (over *780 nm*) [7]. There is a monotonic increase of transmittance in three skin types (slow increase in African) at visible range, and the curve converges at NIR region. The relative work suggested these are according to the melanin absorption [7]. To be specific, the melanin absorption is stronger than hemoglobin absorption in visible range. More elastin and collagen in light skins makes the photon easier collected compared with the dark skin [7]. The transmittance from Lu, L. (2018) is similar with results from Caucasian and Asian skin, which applies a 2 mm porcine skin [18]. As a sample, the porcine skin is extremely similar human skin (*4%* difference in African and 1% difference in Asian as well as Caucasian *@950 nm*) [18]. Secondly, the IV curve of device is shown in Fig. 2 (b) and (c). V_{oc} of skinless is *0.525 V*, and the I_{sc} is *90 μA*. It should be mentioned that the V_{oc} maintains unchanged even with different tissue loss because it is only affected by fabrication process. It is clear to see that the IV curve of Cadence matches that of COMSOL with all skin types. In *950 nm* light operation, the I_{sc} (*32 μA*) of Caucasian is similar with that of Asian, where two curves are overlapped in Fig. 2 (c). The I_{sc} related to African skin is 30 μA, which is slightly smaller than those of the other skins. The IV and PV curves from state of arts were involved to verify the performance in this work [3, 18, 19]. The output power for this work is around *14 μW* with Caucasian and Asian skin, *12 μW* with African skin, which is greater than the other works. One thing needs to be mentioned that the skin profile in this work is from a vivo test, and the skin loss in vivo test is much higher than that in vitro test, which causes more power consumption in this simulation [7]. Eventually, 4-phase charge pump capacitors in power management unit are *90 pF* and tested by *1.1 MHz* frequency in transient analysis. The input of the main charge pump was taken from the startup charge pump which convert from *0.45 V* to *0.9 V*. Alternatively we can configure two photodiodes in series to provide input voltage of 0.9 V and 28 μW at maximum power point. The system provides four voltage outputs with same loads (*10 pF*, *500 kΩ*) in two modes: double boost and super boost, which are shown in Fig. 3 (a) and (b) respectively. The steady-state voltage of double boost mode is *1.76 V*, which is slightly less than the ideal value (1.8 V). As to the super boost mode, ideally (*2.7 V*, *1.8 V*), the simulated upper voltage outputs are *2.53 V*, and the lower voltage outputs are *1.68 V*. As a result, one output of power management (PM) is used to power the implantable applications whilst second output self-powering to the peripheral circuit of PM.

IV. Conclusion

Our simulation results show that the optimum range of operational wavelengths of our PV device are in the Near-infrared range. By harvesting the light energy in NIR range, the amount of harvested energy is sufficient to power a low-power consumption devices such as pacemaker or biomedical sensor. Future work will focus on the different skin types according to age, gender and the different parts of the body that the device will be implanted. We will also consider the effect of changing the incident angle of light on the amount of harvested energy. Then, our implantable device will be optimized by changing the device profiles based on the skin loss.

References

[1] V. Nabaei, R. Chandrawati, and H. Heidari, "Magnetic biosensors: Modelling and simulation," *Biosensors and Bioelectronics,* vol. 103, pp. 69-86, 2017.

[2] B. Shi, Z. Li, and Y. Fan, "Implantable Energy-Harvesting Devices," *Advanced Materials,* vol. 30, no. 44, p. 1801511, 2018.

[3] S. Ayazian, V. A. Akhavan, E. Soenen, and A. Hassibi, "A Photovoltaic-Driven and Energy-Autonomous CMOS Implantable Sensor," *IEEE Transactions on Biomedical Circuits and Systems,* vol. 6, no. 4, pp. 336-343, 2012.

[4] Z. Chen, M.-K. Law, P.-I. Mak, and R. P. Martins, "A Single-Chip Solar Energy Harvesting IC Using Integrated Photodiodes for Biomedical Implant Applications," *IEEE Transactions on Biomedical Circuits and Systems,* vol. 11, no. 1, pp. 44-53, 2017.

[5] K. Agarwal, R. Jegadeesan, Y.-X. Guo, and N. V. Thakor, "Wireless Power Transfer Strategies for Implantable Bioelectronics," *IEEE Reviews in Biomedical Engineering,* vol. 10, pp. 136-161, 2017.

[6] K. O. Htet, J. Zhao, R. Ghannam, and H. Heidari, "Energy-Efficient Start-up Power Management for Batteryless Biomedical Implant Devices," in *IEEE Int. Conference on Electronics Circuits and Systems (ICECS)*, 2018.

[7] S.-H. Tseng, A. Grant, and A. J. Durkin, "In vivo determination of skin near-infrared optical properties using diffuse optical spectroscopy," *Journal of Biomedical Optics,* vol. 13, no. 1, p. 014016, 2008.

[8] A. N. Bashkatov, E. A. Genina, and V. V. Tuchin, "Optical Properties of Skin, Subcutaneous, and Muscle Tissues: A Review," *Journal of Innovative Optical Health Sciences,* vol. 4, no. 01, pp. 9-38, 2011.

[9] G. Vuye, S. Fisson, V. N. Van, Y. Wang, J. Rivory, and F. Abeles, "Temperature dependence of the dielectric function of silicon using in situ spectroscopic ellipsometry," *Thin Solid Films,* vol. 233, no. 1-2, pp. 166-170, 1993.

[10] F. Abelès, "Recherches sur la propagation des ondes électromagnétiques sinusoïdales dans les milieux stratifiés-Application aux couches minces," in *Annales de physique*, 1950, vol. 12, no. 5, pp. 596-640: EDP Sciences.

[11] H. A. Macleod and H. A. Macleod, *Thin-film optical filters*. CRC press, 2010.

[12] X. Li, N. P. Hylton, V. Giannini, K. H. Lee, N. J. Ekins-Daukes, and S. A. Maier, "Multi-dimensional modeling of solar cells with electromagnetic and carrier transport calculations," *Progress in Photovoltaics: Research and Applications,* vol. 21, no. 1, pp. 109-120, 2013.

[13] E. Moon, D. Blaauw, and J. D. Phillips, "Subcutaneous Photovoltaic Infrared Energy Harvesting for Bio-implantable Devices," *Ieee Transactions on Electron Devices,* vol. 64, no. 5, pp. 2432-2437, May 2017.

[14] E. Moon, D. Blaauw, and J. D. Phillips, "Small-Area Si Photovoltaics for Low-Flux Infrared Energy Harvesting," *Ieee Transactions on Electron Devices,* vol. 64, no. 1, pp. 15-20, Jan 2017.

[15] A. Rashidi, N. Yazdani, and A. M. Sodagar, "Fully-Integrated, High-Efficiency, Multi-Output Charge Pump for High-Density Microstimulators," in *2018 IEEE Life Sciences Conference (LSC)*, 2018, pp. 291-294: IEEE.

[16] K. O. Htet, H. Fan, and H. Heidari, "Switched Capacitor DC-DC Converter for Miniaturised Wearable Systems," in *IEEE Int. Symposium on Circuits and Systems (ISCAS)*, 2018, pp. 1-5.

[17] K. Oo Htet, R. Ghannam, Q. H. Abbasi, and H. Heidari, "Power Management Using Photovoltaic Cells for Implantable Devices," *IEEE Access,* vol. 6, pp. 42156 - 42164, 2018.

[18] L. Lu *et al.*, "Biodegradable Monocrystalline Silicon Photovoltaic Microcells as Power Supplies for Transient Biomedical Implants," *Advanced Energy Materials,* vol. 8, no. 16, p. 1703035, 2018.

[19] K. Song, J. H. Han, H. C. Yang, K. I. Nam, and J. Lee, "Generation of electrical power under human skin by subdermal solar cell arrays for implantable bioelectronic devices," *Biosensors & Bioelectronics,* vol. 92, pp. 364-371, 2017.

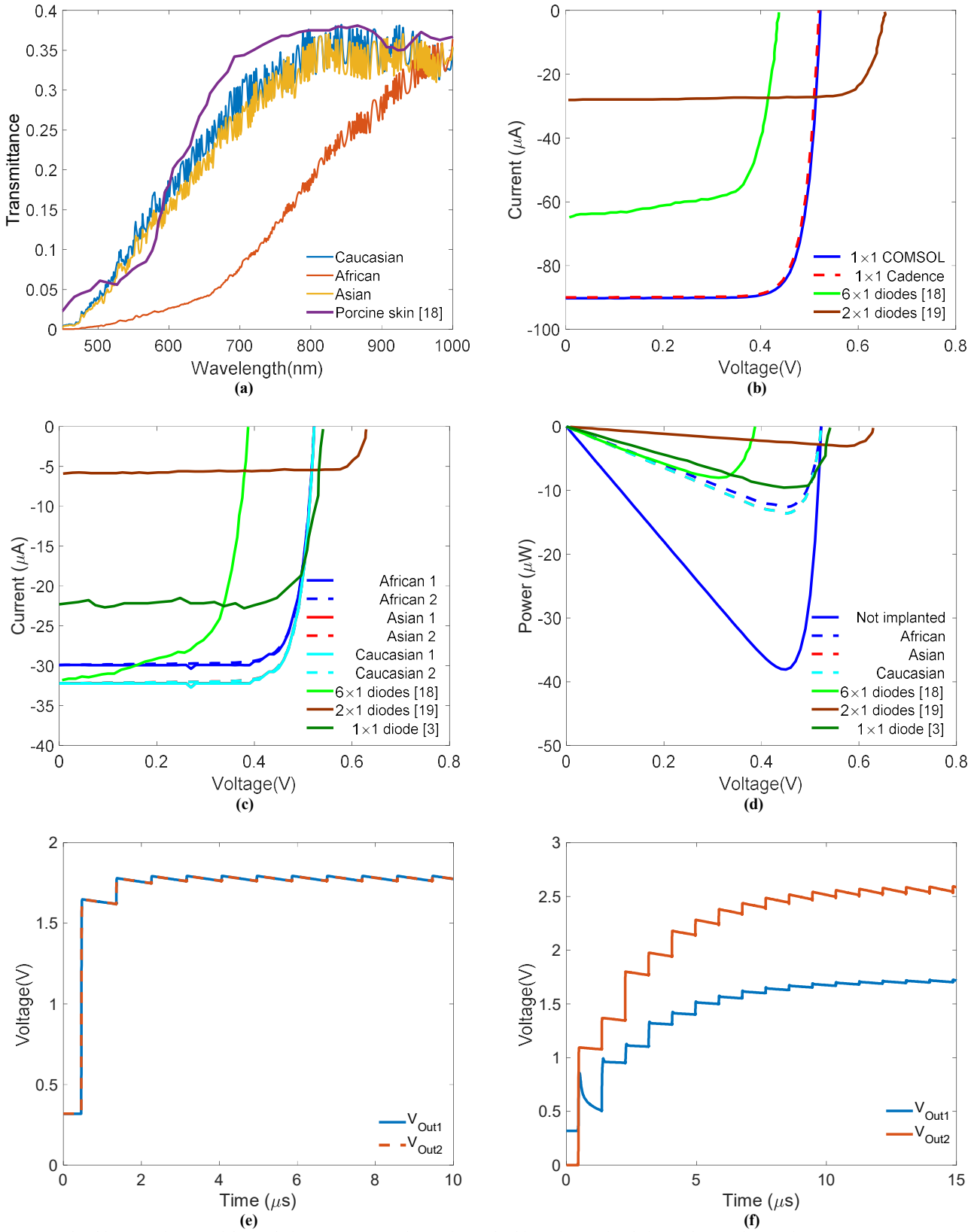

Fig. 2. (a) The skin transmittance of three ethnic groups (Caucasian, Asian and African) in our simulation and transmittance from Lu.L. (2018) [18], where the simulation profile is from the volar forearm of arm and the spectrum range is in visible light and NIR light. (b) The relative IV curve according to full spectrum from this work, Lu, L.(2018) [18] and Song, K.(2017) [19], where 1 means COMSOL simulation results and 2 means the results from Cadence equivalent circuit, (c) The relative IV curve according to skin types of African, Asian and Caucasian with 950 nm wavelength, compared with the IV curve with tissue loss from Lu, L.(2018) [18], Song, K.(2017) [18] and Ayazian, S.(2012) [3]. (d) The relative power generation according to different skin types: African, Asian, Caucasian, skinless compared with the power generation from Lu, L.(2018) [18], Song, K.(2017) [19] and Ayazian, S.(2012) [3]. The output voltage corresponding to transient time from power management unit (e) the double boost (f) the super boost outputs with 10 pF 500 kΩ load.